# Dual-Processing by Abrasive Waterjet Machining – A Method for Machining and Surface Modification of Nickel-Based Superalloy

Zhirong Liao[1,*], Irati Sanchez[1], Dongdong Xu[1], Dragos Axinte[1,2,*], Giedrius Augustinavicius[3], Anders Wretland[4]

[1] Machining and Condition Monitoring Group, Faculty of Engineering, University of Nottingham, UK

[2] Faculty of Engineering, University of Nottingham Ningbo, China

[3] Waterjet AG, Switzerland

[4] GKN Aerospace Engine Systems AB, Sweden

## Abstract

Abrasive waterjet (AWJ) is widely used for machining of advanced (e.g. nickel-based) superalloys as it offers high material removal rates and low cutting temperatures. However, the inadequate surface integrity, e.g. large number of scratches and embedded particles in the machined surface, which would induce severe deteriorations of the materials functional performance, has been one of the greatest issues of the AWJ machining technique. To solve this problem, this research proposed a dual-process abrasive waterjet machining method, whereby two different functions of abrasive waterjet were employed: materials removal (first process) and surface modification (secondary process), hence, to improve the workpiece surface integrity. Two types of entrained particles, i.e. with sharp cutting edges (e.g. garnet) and smooth surfaces (e.g. stainless steel ball), that depending on their kinetic energy density can either cut or modify the workpiece surface respectively, are employed for these the two constitutive processes of the proposed dual-waterjet machining method. A critical standoff distance and inclination angle of the waterjet nozzle has been defined for the surface modification process thus, to eliminate the embedded particles and scratches left by the first cutting process while also introducing a surface strengthening effect. To support this approach, a mathematical model has been proposed for determining the surface modification parameters (e.g. jet feed speed and abrasive flow rate). In-depth analysis of the microstructural and metallurgical alternations of the machined workpiece surface and superficial layer have also been conducted to reveal the mechanisms responsible for the surface damage elimination and surface strengthening. Moreover, a four point bending fatigue test has been conducted to validate the mechanical performance, whereby a significant improvement of the fatigue life on the machined workpiece was achieved when compared with the case that single AWJ cutting method (91%) and conventional machining (34%) are employed. This proves that the proposed dual-processing AWJ machining method is of high efficiency to improve the functional performance of components on a single machine tool platform.

**Keywords:** Abrasive waterjet machining, surface modification, Nickel based superalloy, surface integrity, fatigue

_____

*Corresponding author: Zhirong.liao@Nottingham.ac.uk (Z. Liao), Dragos.Axinte@Nottingham.ac.uk (D. Axinte)

# 1. Introduction

Due to their good combination of mechanical properties at elevated temperatures, Nickel-based superalloys have been widely used for manufacturing components for high-added value industries like aerospace, nuclear and marine (Fang and Toshiyuki, 2017). However, these unique properties also lead to the reduction of their machinability with negative influence on the workpiece surface (Ulutan and Ozel 2011) as high cutting temperature while severe tool wear rate would occur (Axinte et al., 2019), an outcome of the conventional machining process. The poor machinability leads to the deteriorations of the mechanical (e.g. hardness, residual stresses) and microstructural (e.g. recrystallization, phase transformations) properties on the surface and superficial layer, as reported by Liao et al. (2018, 2019a,b). Furthermore, these property alterations can dismiss the strength as well as the creep and fatigue resistance of these unique superalloys compromising their reliability in highly demanding applications (Xu et al., 2020).

Hence, machining of ever-stronger nickel-based superalloys by conventional processes is getting difficult and resources consuming (Shang et al., 2019). Consequently, non-conventional machining operations, which would provide no or less tool wear (Han and Fang 2019) and lower cost (Wang et al., 2019) compared with conventional machining methods, arise as a possible response to this necessity. Among these technologies, abrasive waterjet (AWJ) machining, with its low thermal effect (Folkes 2009) and high material removal rate (Diaz et al., 2019), has received an increasing attention in the machining of difficult-to-cut materials.

On one hand, AWJ machining applies very low cutting forces to the workpiece while the yielded thermal influence is negligible (Wei et al., 2019); hence, no thermal effect on the machined surface is expected. On the other hand, a high machining versatility, simplicity and cutting flexibility can also be obtained as the high pressure jet plume is utilised as a 'cutting tool' (Azarsa et al., 2020). Furthermore, as reported by Axinte et al. (2009), the AWJ machining is also an economical process with high material removal rate at low cost, while it is virtually possible to cut almost any material.

Nevertheless, since the material is removed by a mixture of high velocity waterjet and hard abrasives (e.g. garnet), the machined surface presents a large number of scratches/cutting traces left by abrasive grits (Schwartzentruber et al., 2018). Moreover, Singh and Jain (1995) pointed out that during the AWJ machining process the hard and sharp abrasive particles would also penetrate into the substrate under the high kinetic energy, especially when these grits impact the workpiece at a normal jet impingement angle. Hence, a large number of embedded abrasive grits would occur on the machined surface, particularly when cutting ductile materials. Bound et al. (2010) commented that these grit embedments and scratches can deteriorate the surface roughness and act as stress concentration points which can lead to the reduction of the workpiece mechanical properties and, consequently, contributing to the decrease of their functional performance, especially fatigue. Rivero et al. (2018) reported that a poorer fatigue performance resulted from abrasive waterjet cut process

when compared to the laser cutting process, due to the role of abrasives embedment and scratches acting as crack initiators. This, somehow, limits the spectrum of applications for the AWJ technology when used for the manufacture of aerospace components that require high surface integrity and fatigue performance.

To circumvent this drawback, some researchers have tried to remove or reduce the grit embedment in different ways such as using plain waterjet cleaning, shot peening, grit blasting, ultrasonic cleaning, or even using water soluble abrasives (e.g. ice). However, Kong and Axinte (2009) and Melentiev and Fang (2018) reported that the plain waterjet and ultrasonic cleaning respectively, need long processing time while they could only reach a limited cleaning effect due to low waterjet or ultrasonic energy. With the shot peening and grit blasting process, on one hand, the workpiece needs to be reconfigured to another machine while, on the other hand, the peening/blasting grits would bring another embedment if not configured optimally (Liu et al., 2009). Boud et al. (2014) reported that soluble abrasives can only be used for cutting relatively soft materials while yielding low material removal rates due to the reduced hardness of these abrasives when compared to conventional abrasives (e.g. garnet). Waterjet peening, which employs the cavitation and water droplet impacts generated from high speed waterjet (Chillman et al., 2011), has also been developed for inducing compressive stresses on the workpiece surface but, presents the disadvantage that it cannot clean the embedded abrasive particles. Furthermore, Soyama (2019) reported that whilst a longer processing time is needed for waterjet peening, the enhancement on fatigue strength of this process is much less compared to shot peening and laser shock peening as less strain hardening effect is introduced by the waterjet peening process.

To improve the surface integrity and functional performance of workpiece material under abrasive waterjet cutting, this paper proposed a dual-processing method based on abrasive waterjet machining by employing two different functions of abrasive waterjet, i.e. materials removal and surface modification. That is, depending on the different kinetic energy density of the waterjet plume under various standoff distances (SoD), while a conventional abrasive waterjet cutting (AWJ_Cut) process is firstly applied to cut the material, a secondary in-situ abrasive waterjet surface modification (AWJ_Mod) process is further used for enhancing the surface integrity on the same machine setup. For this, hard and sharp garnet abrasives were employed for the first AWJ_Cut process, while softer and blunt abrasives, i.e. stainless steel ball (SSB), have been used for the secondary AWJ_Mod process whereby a critical standoff distance and inclination angle of the jet plume are defined. To support this approach, a mathematical model was also proposed to determine the surface modification parameters thus, to allow the best surface modification effect along with the removal of the surface microdefects while introducing a surface strengthening effect simultaneously. In-depth surface integrity investigations have been conducted with scanning electron microscope (SEM), energy-dispersive X-ray (EDX), electron back-scattered diffraction (EBSD) and X-Ray diffraction (XRD) to reveal the mechanisms of surface damage elimination and strain

hardening, while the fatigue testing was also performed to validate the material mechanical performance of the proposed dual-process abrasive waterjet machining .

## 2. Dual-process abrasive waterjet machining

### 2.1 Proposed concept

The principle of abrasive waterjet machining is to erode/remove the workpiece material by impact of multiple high velocity (e.g. 300-700 m/s) abrasive particles, enabled by the use of high pump pressure (e.g. ~400 MPa), as shown in Fig. 1(a). In this process, the jet exiting the focusing tube can be generally divided into continuous, open and diffused jet regions under different standoff distances (Chillman et al., 2011) (Fig. 1b). The continuous jet region is close to the focusing tube where the waterjet is still keeping the form of a continuous stream with a high axial dynamic pressure which can be regarded as a solid beam, hence mainly used for controlled depth/through cutting purposes (He et al., 2020). With the increase of the distance from the focusing tube the waterjet beam gets unfocused due to the interaction between the water and the surrounding air, leading to an open jet region with a decreased energy density of waterjet beam. This region can be used for surface modification purposes due to its lower jet kinetic energy density and higher beam diameter, and so, a larger working area. Following the open jet region, the jet is further diffused and its kinetic energy density is substantially reduced hence, it could not modify the surface or sub-surface of the workpiece effectively and is considered as an unusable jet region.
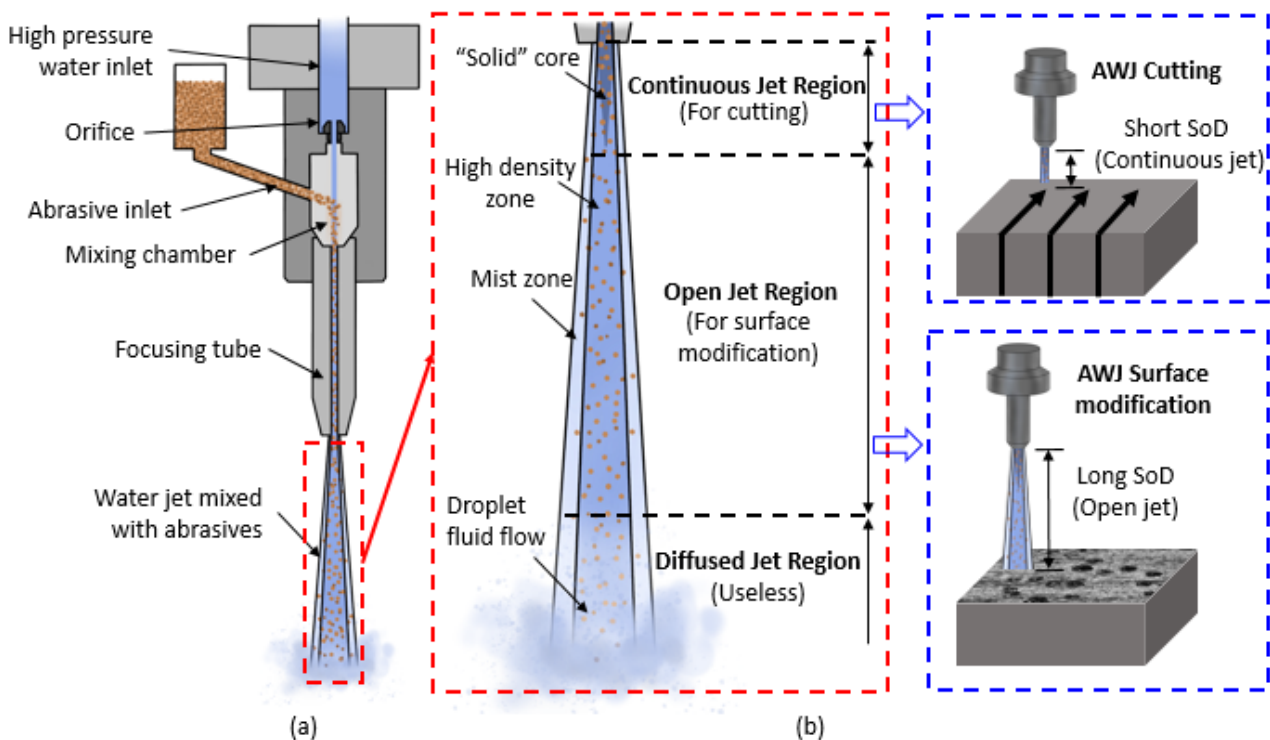


Fig. 1. Schematic explanation of abrasive waterjet machining system (a) and its application in cutting and surface modification under different standoff distances (b) (adapted from Chillman et al., 2011).

Nevertheless, due to the nature of high hardness and sharpness of the abrasives possessing high kinetic energy, these could be easily embedded into the workpiece materials when employing abrasive waterjet machining, especially when cutting ductile materials (e.g. metals), as shown in Fig. 2. These surface defects can generate stress concentrators which could result in reduction of the workpiece fatigue life as high as 30% (Liu et al., 2009); hence, this effect could rise concerns when employed for the manufacture of components that require high surface integrity.
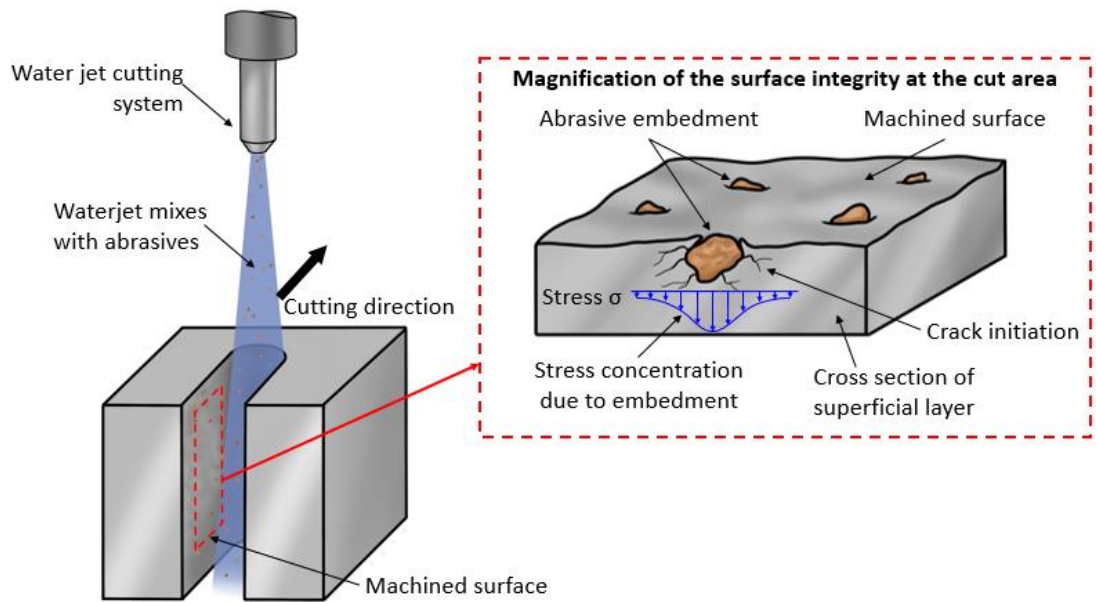


Fig. 2. Abrasive embedment on the side walls of the kerf caused by abrasive waterjet through cutting.

Consequently, it is necessary to investigate on the surface modification of the abrasive waterjet cut workpiece to eliminate these surface defects and increase the surface integrity and eventually to improve the workpiece functional performance. For this, a dual-process AWJ machining method is proposed. As shown in Fig. 3(a), at first a short standoff distance (SoD) is chosen for abrasive waterjet cutting to work within the continuous jet region while garnet abrasive is applied, namely first AWJ_Cut process. Then, a secondary AWJ surface modification process, AWJ_Mod, is developed to treat the machined workpiece surface, whereby a higher value of SoD is chosen to allow the waterjet to work under the open jet region hence less energy intensity is applied, while abrasive media with smooth surfaces (e.g. stainless steel ball) is employed for impinging the workpiece surface instead of cutting. In this process, an inclination angle of 45° of the jet is chosen, which allows a skipping effect of the stainless steel balls when impinging the workpiece surface and therefore, extruding out the existing garnet embedment while avoiding the generation of new embedments, which could occur if the jet impinges at a normal angle. Nevertheless, since an extent of plastic deformation would be generated on the surface due to the stainless steel ball impingement, a strain hardening effect on the workpiece surface would also be expected. Hence, while a specific trajectory that covers the whole machined surface is applied, as shown in Fig. 3 (b), the AWJ_Mod process allows not only the elimination of the grit embedment and microdefects but also the strengthening of the workpiece

surface. Consequently, the proposed dual-process AWJ machining, on the one hand offers the advantage of low cutting force and temperature from AWJ_Cut process, while on the other hand yields an enhanced workpiece surface through the surface modification process.
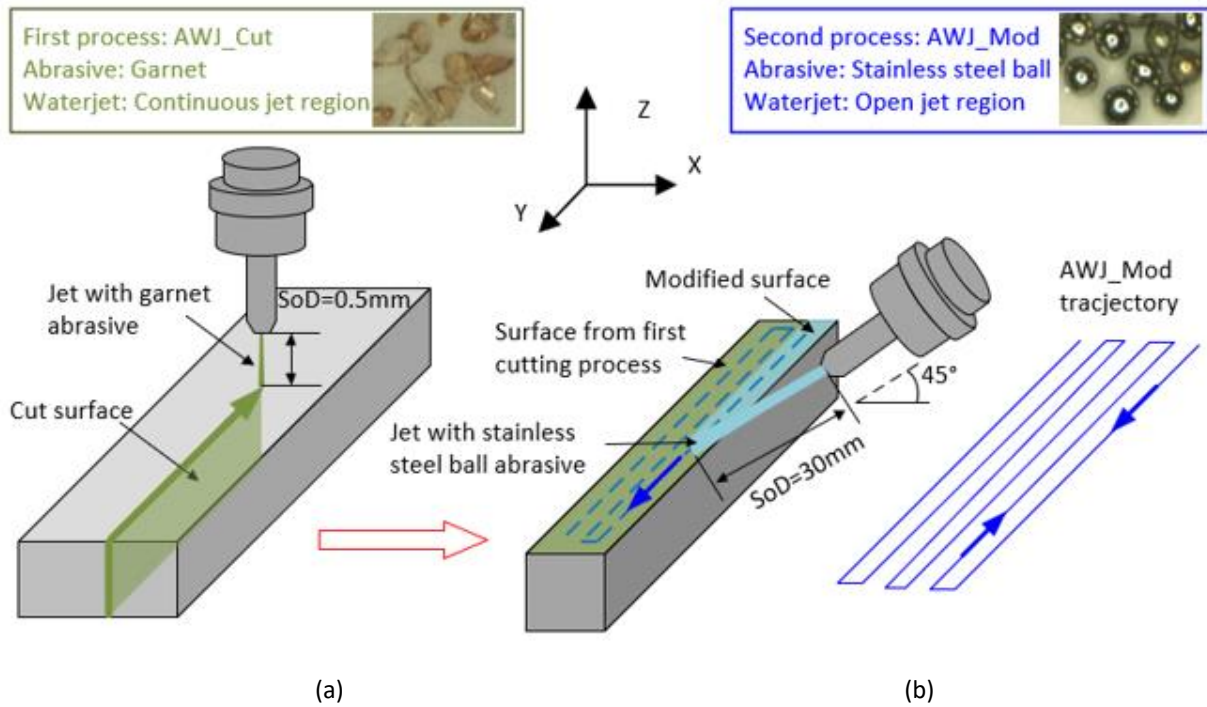


Fig. 3. Proposed dual-process AWJ machining with firstly process of AWJ_Cut for workpiece cutting (a) and secondary process of AWJ_Mod for surface modification (b)

## 2.2 Key issues in dual-process AWJ machining

As shown in Fig. 2, in AWJ_Cut process, to achieve high straightness of the wall kerf profile at different depths of cut, a proper setting up of the process and parameters (e.g. water pumper pressure at 100-400 MPa, jet feed speed at 10-100 mm/min and SoD at 0.5-5 mm) have been tested to achieve the optimised process parameters. While this kerf profile optimisation has also been well documented in previous research (Kong and Axinte 2009), in this paper the undesired outcomes (i.e. grit embedment) are studied with the scope to eliminate them by the secondary process, i.e. AWJ_Mod.

In this condition, in order to ensure robust modification of the entire AWJ_Cut surface, two different factors have to be considered in the secondary AWJ_Mod process:

(i)    To choose a proper region of the jet plume (Fig. 1b) which yields enough energy density that allows the stainless steel balls to scoop the embedded abrasive grits without eroding the surface;

(ii)   To choose appropriate parameters to ensure a full coverage of the entire surface with stainless steel ball impingement.

In this case, an open jet region, wherein the abrasive waterjet mixture has less energy density (i.e. not to erode the material) while the jet plume is wider to reach high surface modification area, has to be determined for the AWJ_Mod application, as shown in Fig. 1(b). While it is difficult to develop an analytical model to decide these three different waterjet regions due to the complex interactions between the waterjet and surrounding air, most researches defined these three regions empirically (He et al., 2020). Hence, in this research a high speed camera (IDT Y4) has been employed to record the shapes of the jet plume at 4500 frames per second (Fig. 4a) which then were post processed by transforming the grey colour scheme to water density percentage. The waterjet machine setup is as described in section 3 when using stainless steel ball as abrasives at the flow rate of 15 g/min.

As shown in Fig. 4(b), it can be seen that under a constant pressure (i.e. 200 MPa) the waterjet is stabilised within the SoD of 0-45 mm, including the continuous jet (0-15 mm SoD) and open jet (15-45 mm SoD) regions, while in the region exceeding 45 mm SoD the jet becomes more misty and leads to a diffused waterjet region. In detail, from the geometry measurement of the jet plume (Fig. 5a) it can be observed that the jet suffers a sudden expansion as exited the nozzle while the width of mist zone increases quickly from 0.1 to 1.2 mm in the continuous jet region. Within the open jet region the width of the mist zone keeps at a stable value (i.e. 1.4-1.5 mm) but it increases dramatically in the diffused jet region (i.e. >4 mm at SoD=65 mm). It is also interesting to find that although the diameter of jet plume (to the outside of the mist zone) varies significantly along the jet direction (Fig. 5a) due to the continuous interactions between the waterjet and surrounding air, this varies very little under different pressures. Specifically, at a constant SoD (e.g. 30 mm), with the increase of waterjet pressure from 100 to 400 MPa the diameter of jet plume only slightly increases from 3.2 to 3.9 mm, as shown in Fig. 5(b).



(a)

(b)
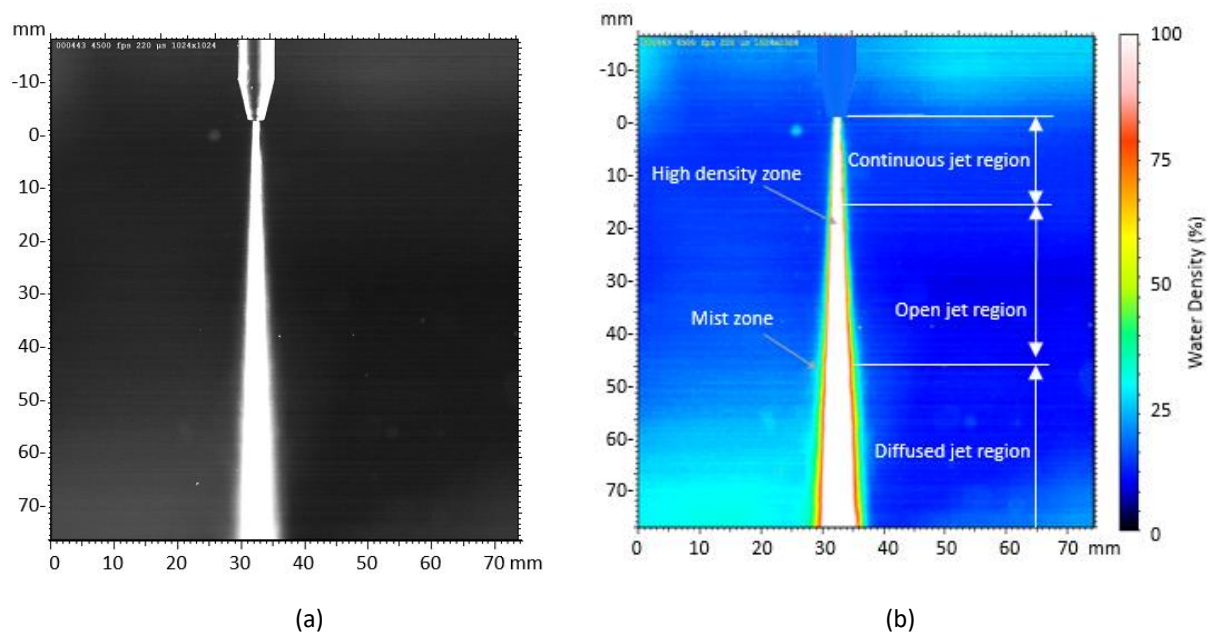
Fig. 4. Geometry analysis of waterjet beam: high speed camera recorded image (a) and post processed with water density percentage (b).

This spreading phenomenon of the waterjet plume not only determines surface modification area but also governs the jet energy density distribution along axial direction. Hence, based on the calibration of the jet geometry the diameter of jet plume ($D_j$, in the unit of mm) can be empirically fit as a function of the standoff distance ($d_{sod}$, in the unit of mm) at a given pressure:

$$D_j = 5 \times 10^{-5}(d_{sod})^3 - 3.8 \times 10^{-3}(d_{sod})^2 + 0.1545 d_{sod} + 1.243 \qquad (1)$$



(a)                                           (b)
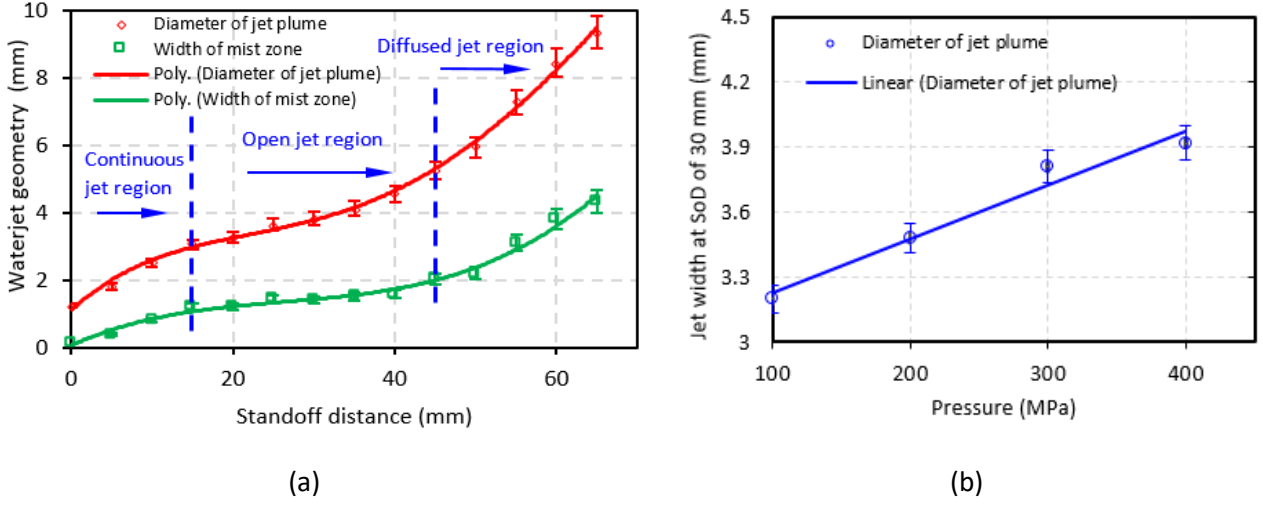
Fig. 5. Waterjet geometry measurement: diameter of waterjet plume and mist zone (a) and diameter of waterjet plume at SoD=30 mm with varied pressure (b); error bars represent 1 standard deviation of 3 measurements.

Hence, to meet the first requirement, i.e. factor (i) choosing a proper jet region with enough energy density to scoop the embedded abrasive grits without eroding the surface, the variation of the energy density along the axial and radial direction needs to be assessed. Based on Chillman's investigation (Chillman et al., 2011), the energy density at the centreline of the jet under a certain standoff distance can be expressed as a function of the diameter of the jet plume:

$$E_j = \frac{13.43(C_D P_s^{3/2} \rho_w^{-1/2} d_n^2)}{(D_j)^2} \qquad (2)$$

where $E_j$ is the energy density at the centreline of the jet plume, $C_D$ is the coefficient of discharge and selected as 0.79 based on (Chillman et al., 2011), $P_s$ the water supply pressure, $\rho_w$ the water density and $d_n$ is the orifice diameter.

Nevertheless, since the jet plume is symmetric about the centre axis, the energy density distribution along the radial direction of the jet can be expressed as (Chillman et al., 2011):

$$E_{j,r} = \left(1 - \left(\frac{r}{R_j}\right)^{1.5}\right)^5 E_j \qquad (3)$$

where $r$ is radial distance from centreline of jet, $R_j$ is the radius of the jet plume at a certain standoff distance.

Based on Eq. (1)-(3) the resulting energy density distribution is plotted as Fig. 6, wherein a decreased value of the energy density with the increase of standoff distance as well the radial distance can be observed. Specifically, it is evident that in the continuous jet region the energy is much more intensive (up to an energy density of 20 kJ/mm²s at the centreline) which can remove the material effectively even with the smooth stainless steel balls, as shown in the SEM observation of the eroded surface (Fig. 6a). However, this energy density decreases dramatically along the axial direction and reaches a 10 times lower value in the open jet region (e.g. 2 kJ/mm²s at the SoD of 30 mm) that the erosion cannot be initiated but only surface impingement occurs. Consequently, considering the open jet region can provide a wide and stable waterjet plume for surface modification, in order to remove the grit embedment as well as to strengthen the workpiece surface the middle area of open jet region (i.e. SoD=30 mm) has been chosen for the AWJ_Mod process.



(a)                                                                                          (b)
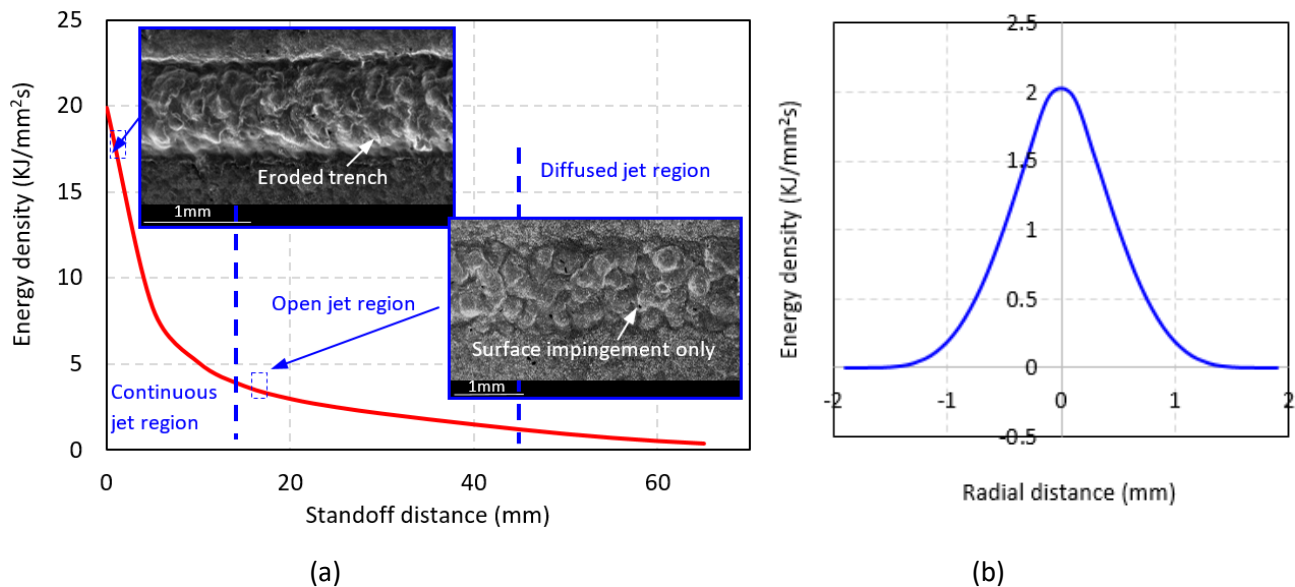
Fig. 6. Energy density along the axial direction in jet centreline (a) and along radial direction at SoD=30 mm (b) at the pump pressure of 200 MPa

Furthermore, while the size of individual stainless steel balls is chosen bigger than the embedded abrasive (i.e. garnet) particles to allow extruding the embedments, the coverage of the entire surface by the impinging stainless steel balls, i.e. factor (ii), also has to be considered. For this, a surface modification ratio can be calculated, which is defined by the sum of all the stainless ball impact areas ($A_b$) divided by the surface that the jet has passed through ($A_w$) as following:

$$R = \frac{A_b}{A_w} \tag{4}$$

To simplify the process, this calculation of the surface modification ratio has been made considering the following hypothesis:

1) The abrasive waterjet mixture is fully composed by stainless steel balls and water, assuming that the air content inside the jet is negligible, when the SoD is short enough to be above the diffused jet region;

2) The size distribution of stainless steel balls is homogeneous;

3) The waterjet-stainless steel ball mixture is homogeneous along the radial direction of the jet plume.

Considering the abrasive flow rate ($m_b$) and the average weight of each ball, which can be achieved by the average ball diameter ($d_b$) with their density ($\rho_b$), the number of balls ejected from the nozzle can be calculated. The average impinging area of a single ball, defined as $A_{bi}$, can also be estimated by measuring the ball impacts with the 3D surface scanner and SEM, as shown in Fig. 7. Consequently, with multiplying the impact area of a single ball by the number of balls, the impact area of all the stainless steel balls ($A_b$) can be estimated as

$$A_b = \sum_i A_{bi} = \frac{6m_b}{\pi(d_b)^3\rho_b}A_{bi} \tag{5}$$

As shown in Fig. 7(b), considering the jet inclination the projected area is an ellipse, hence the jet impact area can be calculated with the trigonometry of the original jet plume diameter at a certain SoD ($D_j$). Consequently, the total area of the surface that the jet has passed through ($A_w$) can be achieved from Eq. (6). The Fig. 7 shows a summarised schematic representation of how the modification ratio, R, was obtained. Consequently, based on the calculation of surface modification ratio the operating parameters, i.e. abrasive flow rate and jet feed speed, can be optimised.

$$A_w = A_{w1} + A_{w2} = \frac{\sqrt{2}}{4}\pi(D_j)^2 + \sqrt{2}V_f D_j \tag{6}$$
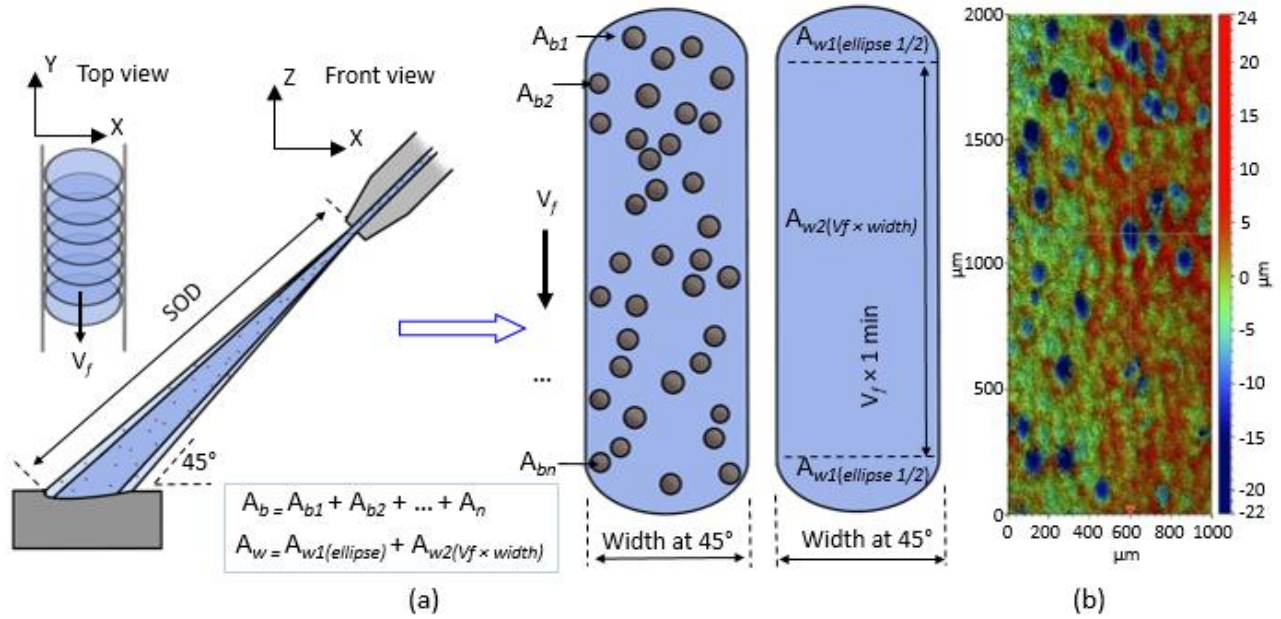
Fig. 7. Schematic representation and quantitative details of the generated jet and impact trench by AWJ_Mod process (a) and the final modified surface (b).

## 3. Experimental procedures

The scope of this research is not only to enhance the waterjet machined workpiece surface quality but also to document and explain how this results in an improved fatigue performance. To evaluate the influence of surface quality obtained from different machining processes upon the component fatigue performance, testing samples (Inconel 718) were first cut to 100 mm x 6 mm x 6 mm by AWJ_Cut process using garnet abrasives (mainly consisting of Al, Si and O) and then modified by the secondary AWJ_Mod process using stainless steel ball (Fig. 8). A Microwaterjet 3-axis machine (Waterjet AG) was used for the experimental work of both the AWJ_Cut and AWJ_Mod processes.

For the AWJ_Cut procedure an orifice of 120 μm diameter and focusing tube of 300 μm diameter have been employed to expel garnet abrasives (220 HPX BARTON, mesh size of 170) with 60 g/min abrasive flow rate. Considering the straightness of the wall kerf and machine capability limitation, a various combinations of process parameters have been tried (e.g. water pumper pressure at 100-400 MPa, jet feed speed at 10-100 mm/min and SoD at 0.5-5 mm) and an optimized waterjet pump pressure of 400 MPa, jet feed speed of 30mm/min and standoff distance of 0.5 mm have be chosen for the first AWJ_Cut process.

To achieve a larger waterjet plume, the secondary AWJ_Mod process has been employed with a 180 μm diameter of orifice and 500 μm diameter of focusing tube while commercial stainless steel balls (AMACAST ES-140) were selected as abrasives (with average diameter of 160 μm) for the surface modification process. A SoD of 30 mm at constant pressure (i.e. 200 MPa) has been selected based on the evaluation in Section 2, while different jet moving velocities (100 - 750 mm/min) and abrasive rates (2-15 g/min) have been tested to achieve the best surface modification effect, as specified in

Table 1. For comparison, plain waterjet cleaning (PWJ_Clean), i.e. without abrasives, has also been conducted with the same setup of AWJ_Mod process.
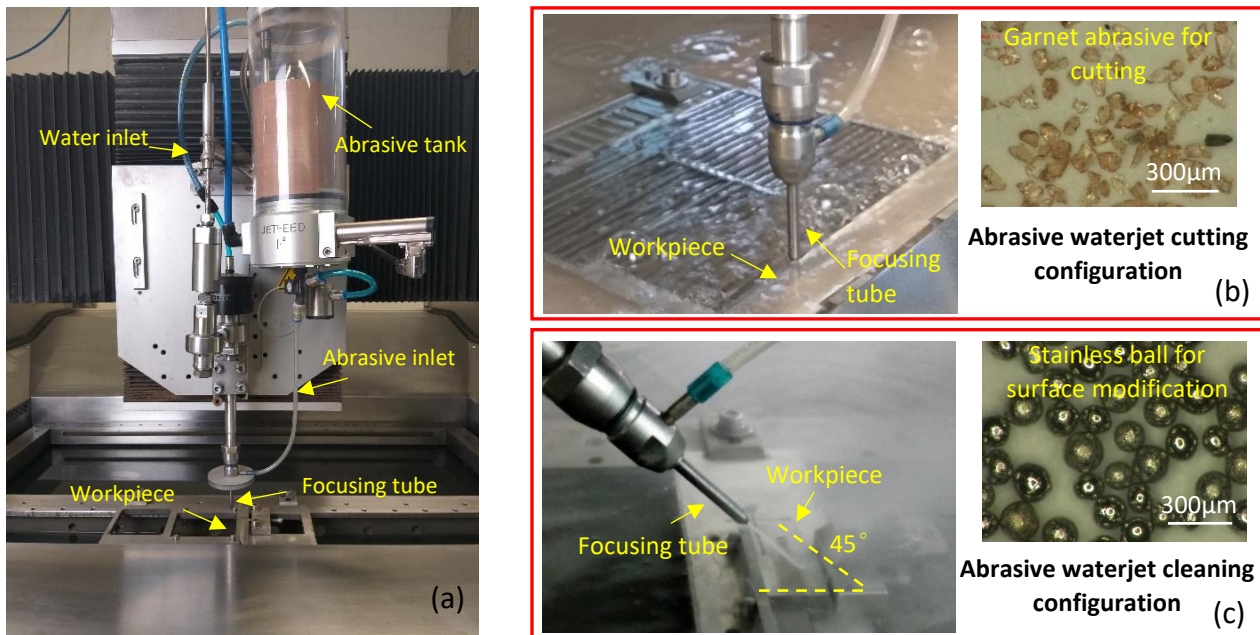


Fig. 8. Experimental setup: Abrasive waterjet machining system (a), configuration for first AWJ_Cut process (b) and secondary AWJ_Mod process (c).

The machined surfaces were measured with the Alicona G5 3D scanner to evaluate their morphology while SEM (FEI Quanta600) incorporating EDX software (BRUKER) and EBSD (Oxford instruments) were employed for evaluating the surface integrity. To understand the surface strengthening effect, residual stresses have also been measured by a Proto XRD with electro etching to evaluate the stress condition in the superficial layer. For further revealing the influence of surface modification effect on the fatigue performance, a four-point bending fatigue test was conducted on the samples from AWJ_Cut and AWJ_Mod processes with an Instron 8801 testing machine. The sinusoidal cyclic load was applied with a frequency of 5 Hz and stress amplitude ratio of 0.1, whereby the maximum and minimum stress were set as 100% and 10% of the yield stress (1250 MPa) respectively. The support span was setup as 80 mm and load span as 40 mm, as shown in Fig. 9.
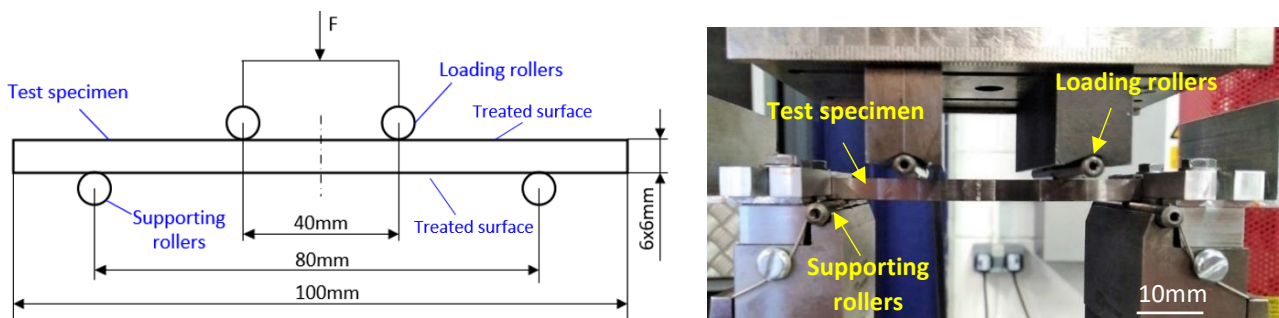


Fig. 9. Four points bending fatigue test: schematic illustration (a) and experimental setup (b).

# 4. Results and discussion

## 4.1. Surface damage induced by AWJ_Cut process

In order to examine the surface damage of AWJ_Cut samples, a SEM and EDX mapping were performed on the centre of the sample to obtain the microstructure of workpiece surface, as shown in Fig. 10. It can be seen that while the SEM image gives only the geometrical information (e.g. scratch marks), the embedment of garnet abrasives is more conspicuous to be revealed by EDX analysis as the main chemical characteristics of garnet abrasive (i.e. Si and Al) is not contained in the substrate material (i.e. Inconel 718). Not surprisingly, a large amount of scratch marks and embedments have been detected on the workpiece surface generated by AWJ_Cut due to the high-velocity impacts of the hard and sharp garnet abrasives. However, it is interesting to observe that these embedments are much smaller (~30 µm) than the original abrasives (~90 µm), indicating a severe fragmentation of the abrasive particles under the high kinetic energy impact. Nevertheless, the fragmented smaller abrasives are in general sharper and more perceivable to jet flow turbulence hence easier to penetrate the substrate material and subsequently embedded into the machined surface (Melentiev and Fang, 2018). More interestingly, the size of the scratch mark is found comparable to that of embedments, which is more likely generated by the sharp edge of larger particles as they have a higher tendency to orient themselves with a sharp corner towards the jet direction (Hadavi et al., 2015) while after scratching they are also easier to be carried away by the high pressure waterjet flow due to the higher volume and mass. It is important to note that both these scratches and abrasive embedments may generate stress concentrations and acts as initiators and propagators when loading the workpiece; hence they should be eliminated with a secondary process of AWJ_Mod.



(a)                          (b)
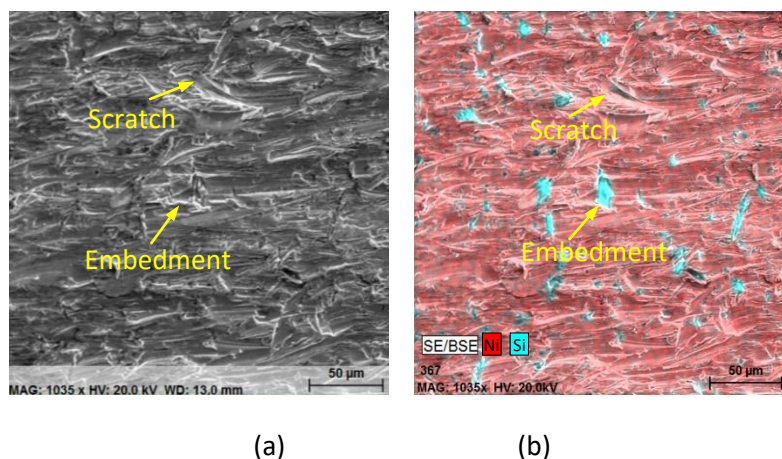
Fig. 10. The SEM (a) and EDX (b) mapping of AWJ_Cut surface showing a large number of scratches and abrasive embedments.

## 4.2 Surface Modification effect of AWJ_Mod process

### 4.2.1 Surface analysis at macro level

In order to find the optimum parameters for the surface modification, i.e. jet feed speed ($V_f$) and abrasive (steel balls) flow rate ($m_b$), Table 1 presents the estimated surface modification ratio ($R$) at the selected pressure (i.e. 200 MPa) with different modification parameters. Based on the evaluation from Eq. (4)-(6) as well as the experimental observation of jet plume geometry (Fig. 4 and 5), the waterjet impact area ($A_w$) and total stainless steel balls impact area ($A_b$) can be achieved, hence the surface modification ratio ($R$) can be calculated. As shown in Table 1, it is evident that the surface modification ratio increases with the rising abrasive flow rate due to the higher particle impinging density, while this value decreases with the increase of the jet feed speed due to the shorter jet dwell time. This ratio gives a quantified indication of the surface modification efficiency hence, it can be used to inversely determine the parameters to achieve a full coverage of the modified surface. Nevertheless, further experimental analysis will also be conducted in the following surface analysis to validate this calculated surface modification efficiency.

Table 1. Surface modification ratio under different parameters

| No. | Jet speed $V_f$ (mm/min) | Abrasive flow rate $m_b$ (g/min) | Total ball impact area $A_b$ (mm$^2$) | Jet impact area $A_w$ (mm$^2$) | surface modification ratio R ($A_b/A_w$) |
|-----|-----|-----|-----|-----|-----|
| 1 | 750 | 2 | 126 | 3428 | 0.04 |
| 2 | 250 | 2 | 126 | 1173 | 0.11 |
| 3 | 250 | 4 | 251 | 1336 | 0.19 |
| 4 | 250 | 7 | 441 | 1336 | 0.33 |
| 5 | 200 | 7 | 441 | 1080 | 0.41 |
| 6 | 100 | 7 | 441 | 569 | 0.78 |
| 7 | 100 | 15 | 945 | 569 | 1.66 |

For this, the 3D morphology of the samples from different processes has been measured, as shown in Fig. 11, whereby the surface damages and modifications can be examined at a macro level. It is interesting to find that while scratch marks are the main defects on the AWJ_Cut workpiece (Fig. 11a), a secondary plain waterjet cleaning (PWJ_Clean) does not have a significant alteration of the scratch marks at the macro scale (Fig. 11b). This is because only the water droplets are acting as "abrasive" media in plain waterjet cleaning process, which are soft and do not possess enough energy to generate plastic deformation/modification of the relatively hard workpiece material. On the contrary, a series of visible impinging craters can be observed on the surface processed by the AWJ_Mod method, as shown in Fig. 11 (c)-(f), due to the high impact energy of the accelerated stainless steel

ball. These craters, indicating a severe plastic deformation on the target surface, not only eliminate the stress concentrations caused by the scratches left by previous process (AWJ_Cut) but can also introduce high compressive stresses that result in a surface strengthening effect.

Nevertheless, when a proper surface modification ratio (i.e. R=1.66) is applied, a significant surface modification effect can be generated by AWJ_Mod process, whereby a large number of stainless steel balls are delivered by the waterjet to impinge the surface, as shown in Fig. 11(f). However, when insufficient stainless steel balls are delivered, the surface could not be modified effectively, as shown in Fig. 11(c) and (d), where a large scratched area are left on the surface due to the low surface modification ratio (i.e. R = 0.04 and 0.11). These surface morphology observations are coincident with the surface modification ratio calculation results from Table 1, whereby the optimum coverage of the surface modification can be achieved when the surface modification ratio R is larger than 1. A more detailed analysis of the cleaning effect on abrasive embedment will also be analysed by SEM observation at micro level in the following investigation.
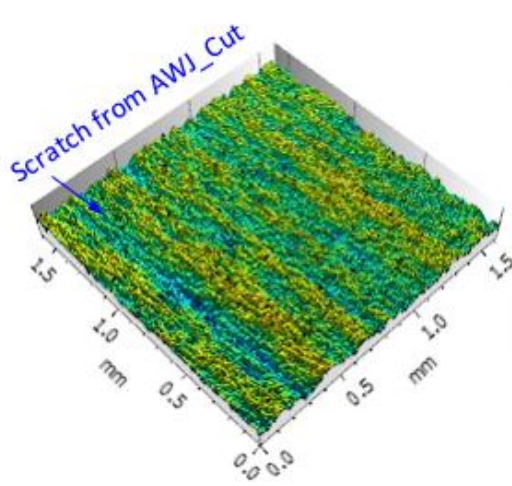


(a) AWJ_Cut surface
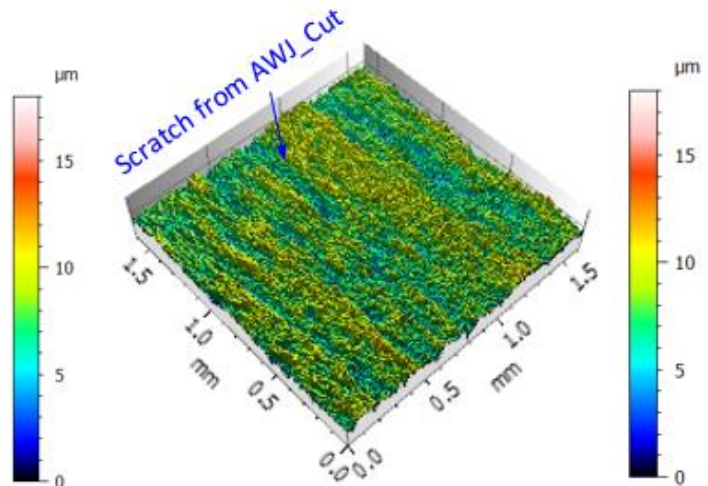
(b) Plain WJ cleaned surface
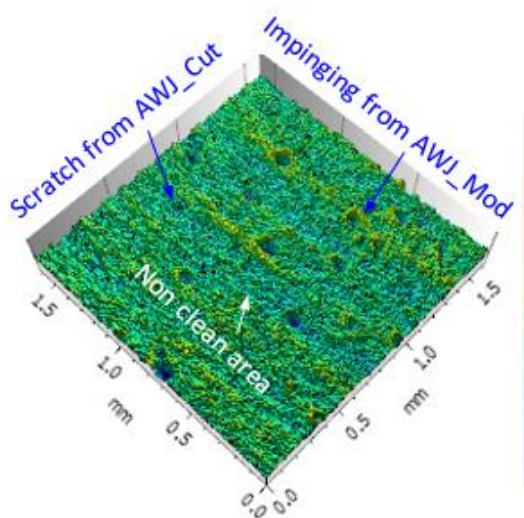
(c) AWJ_Mod surface at R=0.04

(d) AWJ_Mod surface at R=0.11

(e) AWJ_Mod surface at R=0.78        (f) AWJ_Mod surface at R=1.66
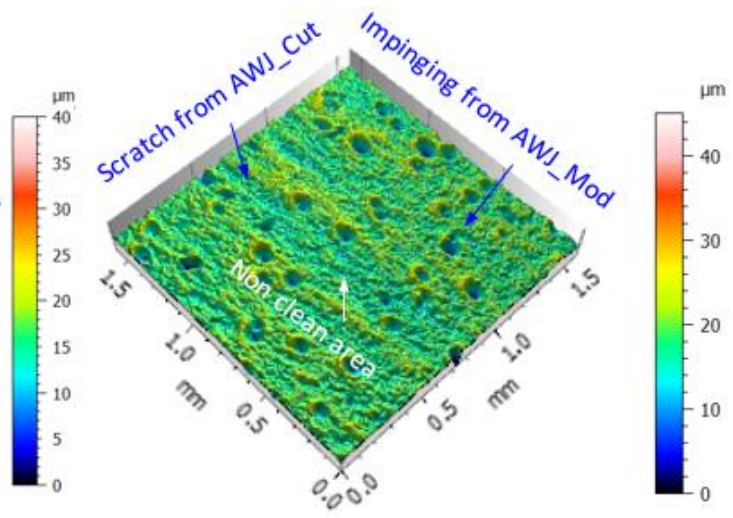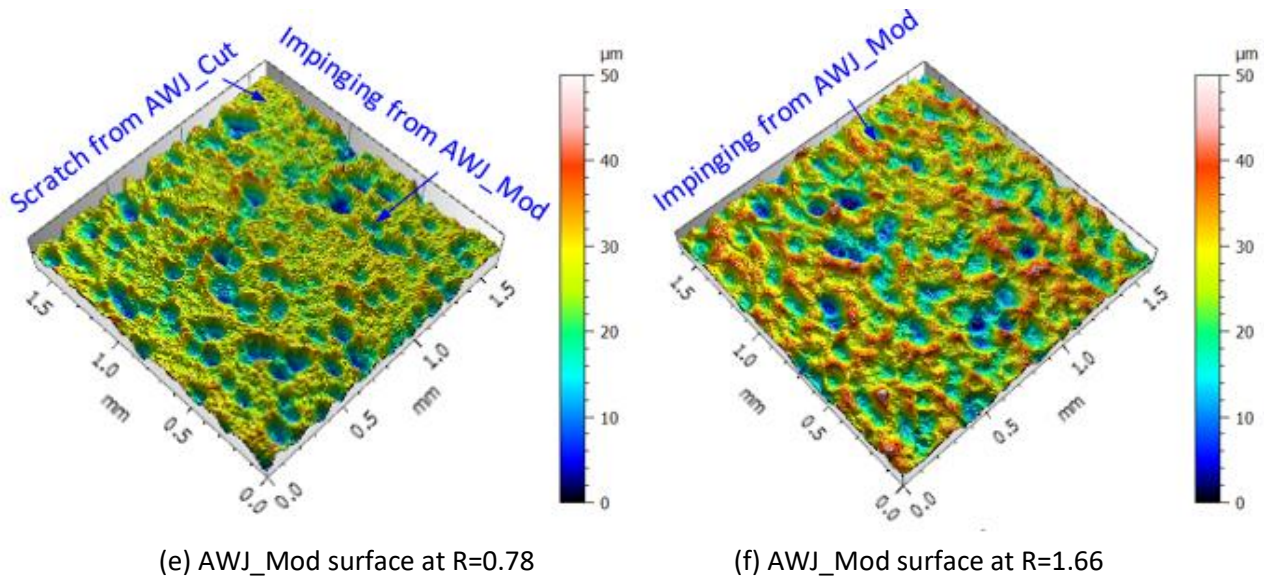
Fig. 11. Surface morphology from different processes showing a better surface modification effect at macro scale under higher surface modification ratio

### 4.2.2 Surface analysis at micro level

While the 3D morphology observation (Fig. 11) shows the surface modification effect at the macro level, the abrasive embedment cleaning cannot be evaluated with this method as the embedment occurs at a micro level. Hence, the SEM and EDX mapping are applied on the centre of the samples under different surface modification conditions (Fig.12–16) to investigate their governing mechanisms.

Interestingly, from the micro observation of the plain waterjet cleaned workpiece, as shown in Fig. 12, it can be found that whilst the scratches still exist, there is also a large number of embedments left on the surface. This is because while abrasive embedments are stuck into the workpiece material, the delivered water droplets are soft and cannot transfer enough energy flux to completely remove these embedments from workpiece material, hence demonstrating a low cleaning efficiency. Furthermore, some voids have also been observed that are related to the spots where the embedments have been removed; Nevertheless, the high-velocity droplets can neither induce plastic deformations nor substantially remove the target material and, therefore, a high density of scratch marks are still left on the workpiece surface that can still cause stress concentrators and potentially initiate/propagate the cracks.

(a)                                    (b)
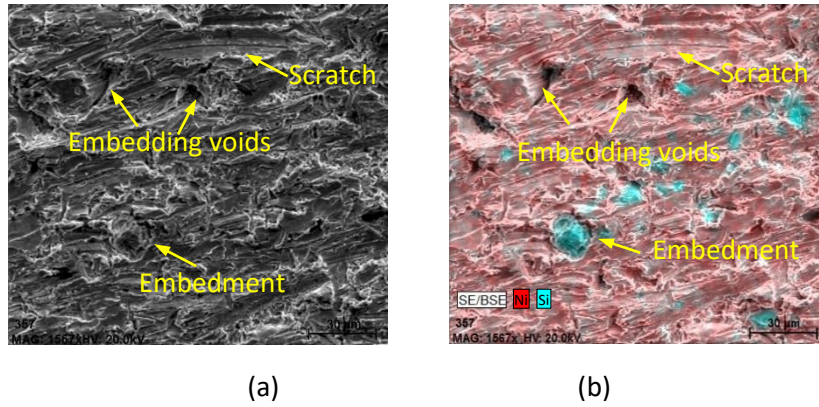
Fig. 12. SEM (a) and EDX (b) mapping of plain water cleaned (PWJ_Clean) surface showing abrasive embedments, voids and scratches.

On the contrary, when applying AWJ_Mod process with an inclination angle (i.e. 45°), a distinct plastic extrusion effect from stainless steel ball impinging can be generated on the workpiece surface, hence pushing/scooping out the embedded garnets abrasives from the substrate while also eliminating the scratch marks effectively, as shown in Fig. 13. However, due to the lack of abrasive flow when applying a high jet feed speed (i.e. low dwell time), a low surface modification ratio (i.e. R=0.04) is yielded. This results in a large area of unmodified surface left on the workpiece whereby the embedments and scratches still exist, as shown in the top surface and cross section observation. Note that the cross section mapping (Fig. 13 c) was randomly selected and does not correspond to the same area from Fig. 13 (b).







(a)                                    (b)                                    (c)
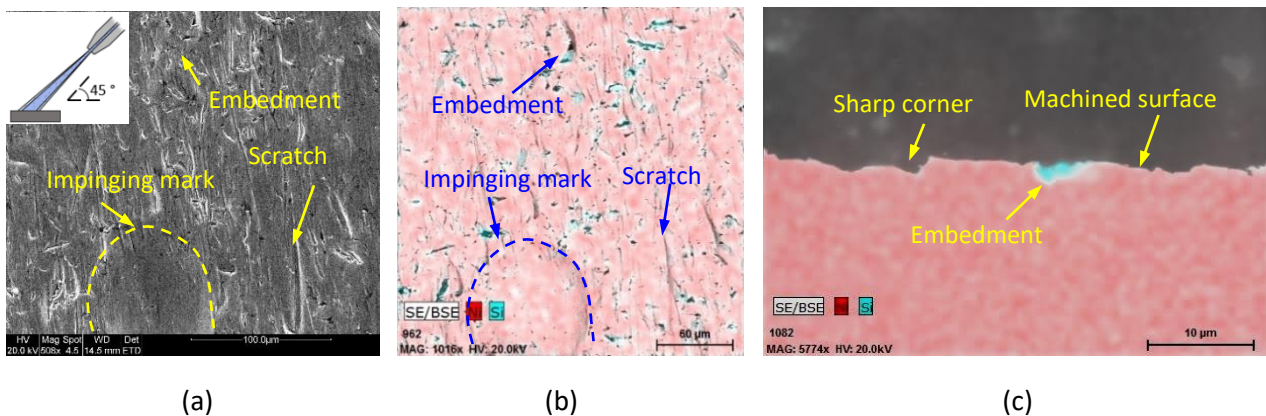
Fig. 13. SEM (a) and EDX (b) mapping of the surface and cross section (c) from the AWJ_Mod workpiece showing that both modified and abrasive contaminated areas exist when conducting with low surface modification ratio (R=0.04).

As discussed in the previous section, to reach a full coverage of the modified surface from stainless steel ball impinging, an increase of the surface modification ratio is needed by raising the abrasive flow rate while reducing the jet feed speed. Fig. 14 shows a proper modified surface under a high modification ratio (i.e. R=1.66), whereby a high density of impinging mark/plastic deformation has been generated on the workpiece surface and leads to a significant surface modification. In this case, as shown in the surface and cross section observations, neither the abrasive embedments nor the

scratch marks/sharp corners are left on the modified surface. Hence, with AWJ_Mod process not only a shot peening but also a scooping effect of the embedments from the AWJ_Cut process can be achieved.



(a)                                    (b)                                    (c)
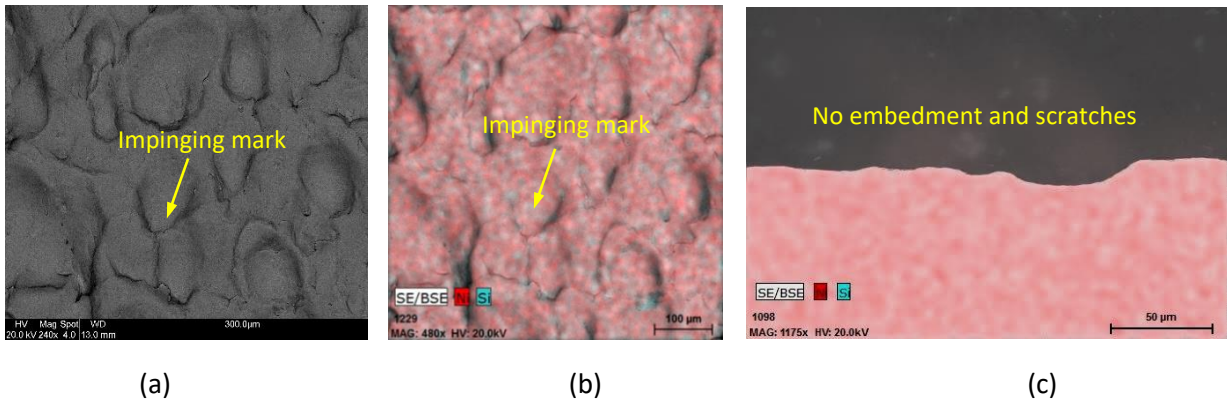
Fig. 14. SEM (a) and EDX (b) mapping of the surface and cross section (c) from the AWJ_Mod wokpiece under a high surface modification rate (R=1.66) showing the modified surface with a high density of impinging mark.

However, while an inclined angle of 45° has been chosen as the example of AWJ_Mod, the query could arise why the jet does not impinge the workpiece under a normal direction but with an inclination angle. From Fig. 15 where the workpiece surface is impinged at a 90° jet angle, it is evident that the garnet abrasive embedments cannot be extruded from the surface (Fig. 15 a and b); on the contrary, they are further pushed into the subsurface under a high plastic deformation due to the hammering effect from the accelerated stainless steel balls. Nevertheless, as the stainless steel balls strike the workpiece surface perpendicularly, a fragmentation of stainless steel ball can also occur which would penetrate into the workpiece material with its high kinetic energy, as shown in Fig. 15 (c) and (d). Hence, AWJ_Mod at a normal angle to the workpiece would not be preferred as a proper surface modification method.



(a)                                    (b)

18
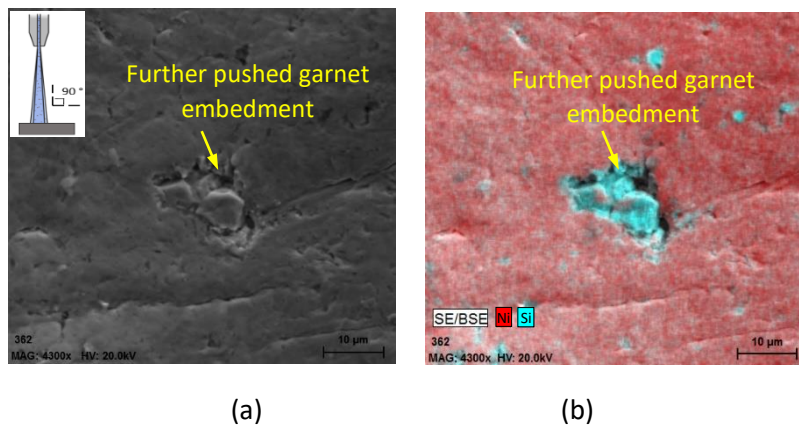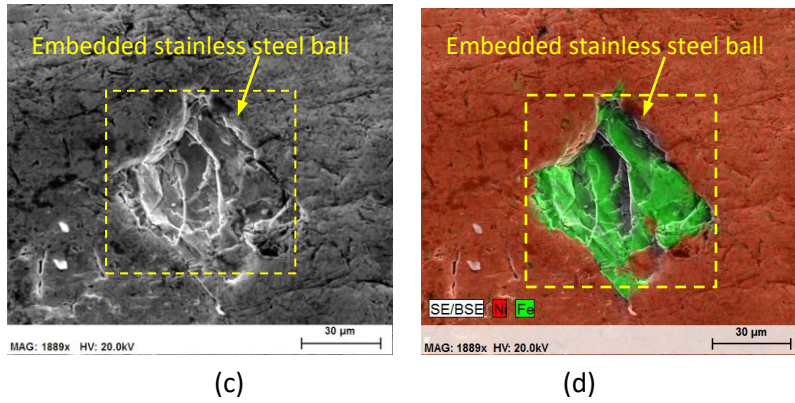
Fig. 15. SEM (a) and (c) and EDX mapping (b) and (d) of the surface from the AWJ_Mod with a normal impacting angle showing the garnet and stainless steel ball embedment.

Consequently, different from normal jet impingement angle, when an inclination angle (i.e. 45°) is applied, the accelerated stainless steel ball can produce a slant plastic extrusion to push out the embedded garnets abrasives while without crack the ball itself. Moreover, this impinging effect supports not only to the extrusion of the abrasive embedments but also eliminates the stress concentrators or small cracks induced by the scratching effect of sharp garnet abrasive, through plastically deforming these micro defects. The observation from AWJ_Mod surface (Fig. 16a and b) shows a clear extrusion effect from the inclined impinging of the stainless steel ball with a high plastic deformation. Hence, the surface modification mechanism from AWJ_Mod can be illustrated from Fig. 16 (c) including three steps: (i) the stainless steel ball impinges the workpiece with high kinetic energy and generates a localised severe plastic deformation on the surface; (ii) the ball keeps on moving in X direction with the residual momentum and levers up the embedded abrasives; (iii) with the residual kinetic energy the stainless steel ball moves upwards and extrudes the abrasive while keeps on deforming the material until it loose contact with the workpiece surface.
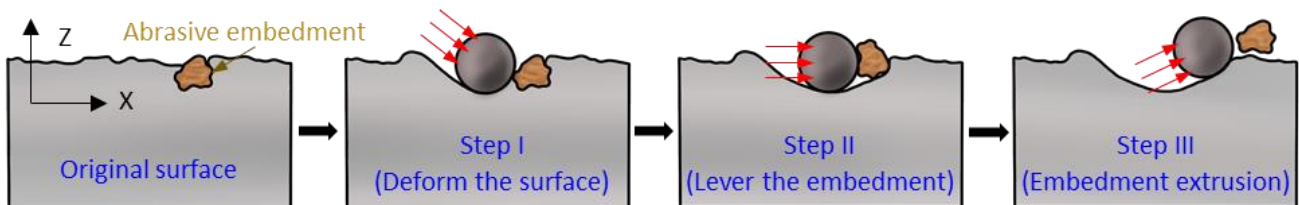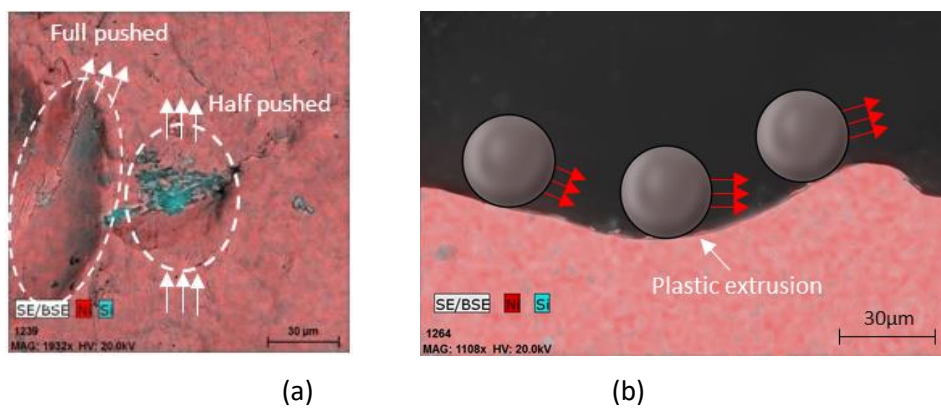
Fig. 16. EDX mapping of the surface (a) and cross section (b) proving the scoping effect of the embedments, a schematic explaining the steps that governs the surface modification mechanism by AWJ_Mod (c).

## 4.3. Strain hardening analysis and fatigue performance

In order to identify the material strengthening mechanism induced by the AWJ_Mod process, the inverse pole figures (IPF) from EBSD mapping and its microstructural local misorientation (LMO) were obtained, as shown in Fig. 17. Surprisingly, there is no clear grain refinement layer found in both AWJ_Cut and AWJ_Mod surface even though high impact energy has been transferred to the workpiece. This is different from previous observation on AWJ_Cut of pure Ni (Mieszala et al., 2017) and impact of pure iron samples (Tumbajoy-Spinel et al. 2018) where large number of grain refinement has been observed from the superficial layer. This is possibly due to the higher strength and multiphase crystalline structure (i.e. high volume fractions of γ'' phase stops the dislocation accumulation) of Inconel 718 that make it more difficult to recrystallise. However, from the local misorientation map (Fig. 17b and d) where small orientation changes (i.e. 5° subgrain angle) in the lattice have been calculated, it can be seen that a high extent of microscale lattice strain was generated on the superficial layer (~40 μm thickness) of AWJ_Mod workpiece due to the severe plastic deformation. On the contrary, in the AWJ_Cut workpiece much less microscale lattice strain has been observed (~5 μm thickness), indicating a lower dislocation density and strain hardening effect. Hence, this high lattice strain in AWJ_Mod surface specifies the strengthening effect from the stainless steel ball impingement which would expect a better materials performance.



(a)                                                    (b)
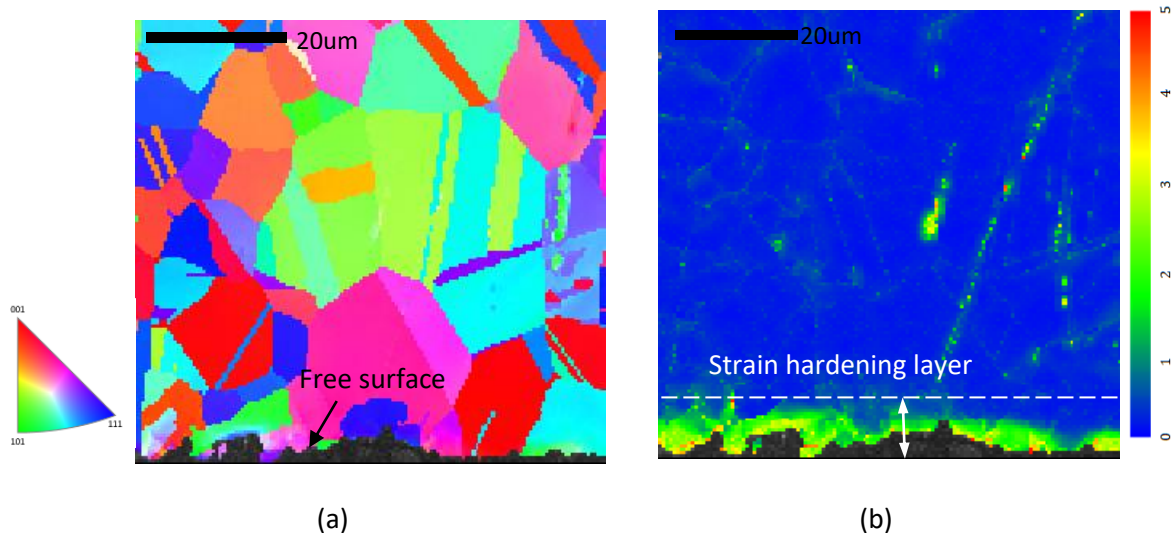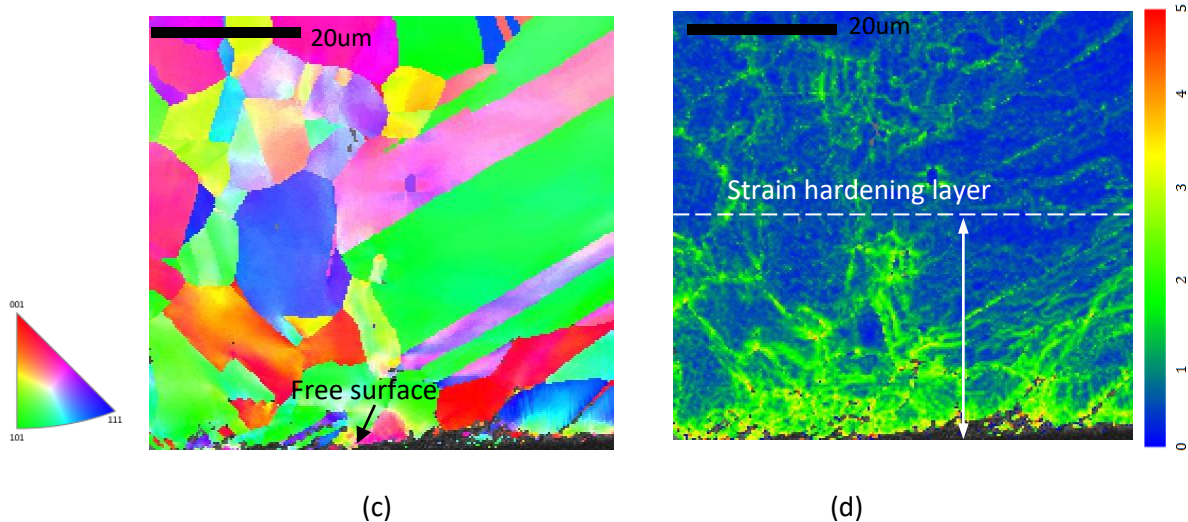
Fig. 17. EBSD IPF images and local misorentation maps of the subsurface from AWJ_Cut (a), (b) and AWJ_Mod (c), (d) processes.

The residual stress beneath the cut surface from different waterjet machining processes has also been evaluated to understand the surface strengthening effect, are shown in Fig. 18. For a comparison with the industrial process, a benchmark, i.e. conventional milled workpiece, that had been machined with a semi-finishing condition (i.e. cutting speed at 35 m/min, feed rate at 0.016 mm/tooth, and cutting depth at 0.05 mm, with flood cutting fluid applied), has also been tested. It is interesting to find that although the conventional machining shows a tensile effect (max. 50 MPa) in the normal (to tool feed) direction, a slightly higher compressive residual stress (max. -450 MPa) is reached in feed direction compared with the AWJ_Cut workpiece. As the residual stress in conventional milling process results from a combination of thermal and mechanical effects, the tensile stress in normal direction is possibly due to the specific milling tool geometry that generates less mechanical compression effect in this direction, whereby the thermal influence (tensile stress) dominates the residual stress condition on the machined surface. More interestingly, while a much higher compressive residual stress (max. -1200 MPa) from the AWJ_Mod workpiece has been achieved, the plain waterjet cleaning workpiece shows a comparable compressive residual stress amplitude to AWJ_Cut process at a lower level (max. -250 MPa). Hence, considering the high compressive residual stress outcome combined with the embedment cleaning effect, an improved functional performance (i.e. fatigue) of the machined nickel based superalloy could be expected from the AWJ_Mod process.
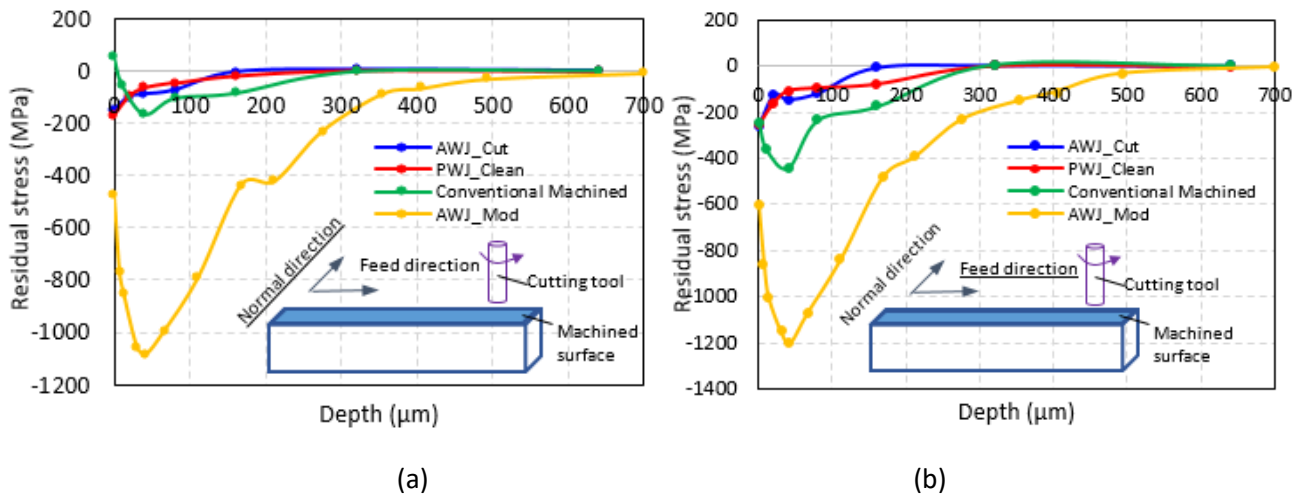
Fig. 18. Residual stress profile from different processes at normal direction (a) and feed direction (b).

To validate their fatigue performance, a four-point bending fatigue test was also conducted on the proposed dual-process abrasive waterjet machined samples and compared with single AWJ_Cut as well as the bench mark (i.e. conventional machining) samples, where the results of fatigue life can be seen in Fig. 19. It is not surprising that the fatigue life of AWJ_Mod samples is much longer than both the conventionally machined (34%) and AWJ_Cut (91%) samples due to the elimination of grit embedments and scratches as well as the increased level of compressive residual stresses. On the other hand, the AWJ_Cut workpiece shows a lower fatigue life compared with the conventional machining (30%) although there is a surface tensile stress in the normal direction of the conventional machined workpiece. This is due to the surface contamination and stress concentration of the AWJ_Cut sample, whereby a large number of abrasive particle embedments and scratches exist, which could initiate and propagate the cracks during the fatigue test. This is consistent with the observations from surface integrity and residual stress in previous sections, and establishes a potential application of abrasive waterjet machining for the safety critical industry. It is also interesting to note that in presented study the surface roughness does not have important influence to the fatigue life although the AWJ_Mod workpiece yields a much rougher surface compared with the other two. This is because of the significant improvement on the surface integrity and strain hardening effect of the AWJ_Mod workpiece as presented in the foregoing discussion.
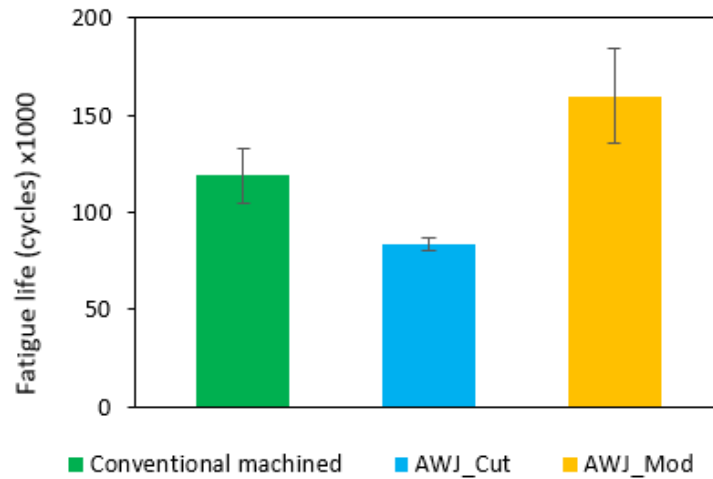
Fig. 19. Fatigue life of machined samples from different processes, error bars represent 1 standard deviation of 5 tests.

## 5. Conclusions

Abrasive waterjet machining is an encouraging method for machining the difficult-to-cut materials with its advantages of high material removal rate and low cutting forces as well as negligible thermal influence. However, the induced mechanical microdefects, i.e. abrasive embedment and scratches, raise the concern for its application in safety critical applications. In this paper, a dual-process abrasive waterjet machining is proposed for the high surface integrity application, whereby a first process of AWJ cutting and second process of AWJ surface modification are employed with different abrasives and waterjet regions applied. In-depth analysis of the modified surface and superficial layer from both the macro and micro scales have also been conducted to reveal the mechanisms responsible for the surface damage elimination and surface strengthening. The experimental validation shows a promising surface modification from AWJ_Mod process in respect to the surface integrity and fatigue performance. The main finding of the paper can be summarised as follows:

- The AWJ_Cut process generates significant abrasive embedment and scratches on the machined surface due to the penetration of the hard and sharp abrasive particles with high kinetic energy density under continuous jet region. The proposed AWJ_Mod process can eliminate these microdefects by impinging the surface with stainless steel balls under an inclination angle and open jet region.

- When a normal jet impingement angle is applied in AWJ_Mod process, the garnet abrasive embedment cannot be removed but further pushed into the subsurface, while the new embedment can also be induced due to the fragmentation of stainless steel balls. With plain waterjet cleaning, a number of voids left from the removed embedments have been observed while there are also a certain number of embedments and scratches that cannot be removed due to the low impinging efficiency.

- To ensure a completed modification in AWJ_Mod process a mathematic model is proposed for predicting the surface modification ratio thus to achieve the optimum parameters. A high surface modification ratio, e.g. R>1, by combining a low jet feed speed and high abrasive flow rate, leads to an effective surface modification, while a low R leads to insufficient stainless steel ball delivered to the surface.

- A three steps surface modification mechanism is proposed of AWJ_Mod process, including the localised plastic deformation, abrasives embedment leverage and extrusion stages. This leads not only to the abrasive embedment extrusion, but also to a surface strengthening effect, i.e., 8 times larger in strain hardening and 5 times higher in compressive stress than AWJ_Cut sample.

- The proposed dual-process AWJ machined sample shows a much higher fatigue life compared with the conventional machined (34%) and AWJ_Cut (91%) samples, due to the cleaning effect of embedment and scratches as well as the high density of plastic deformation generated on the modified surface, hence establishes a potential application in safety critical industry.

## Acknowledgement

## Reference

Axinte, D. A., J. P. Stepanian, M. C. Kong, and J. McGourlay. "Abrasive waterjet turning—an efficient method to profile and dress grinding wheels." International Journal of Machine Tools and Manufacture 49, no. 3-4 (2009): 351-356.

Axinte, D., Guo, Y., Liao, Z., Shih, A.J., M'Saoubi, R. and Sugita, N., 2019. Machining of biocompatible materials—Recent advances. CIRP Annals, 68(2), pp.629-652.

Azarsa, E., Cinco, L., & Papini, M. (2020). Fabrication of high aspect ratio free-standing structures using abrasive water jet micro-machining. Journal of Materials Processing Technology, 275, 116318.

Boud, F., C. Carpenter, J. Folkes, and P. H. Shipway. "Abrasive waterjet cutting of a titanium alloy: The influence of abrasive morphology and mechanical properties on workpiece grit embedment and cut quality." Journal of Materials Processing Technology 210, no. 15 (2010): 2197-2205.

Boud, F., J. W. Murray, L. F. Loo, A. T. Clare, and P. K. Kinnell. "Soluble abrasives for waterjet machining." Materials and Manufacturing Processes 29, no. 11-12 (2014): 1346-1352.

Chillman, A., Hashish, M., & Ramulu, M. (2011). Energy based modeling of ultra high-pressure waterjet surface preparation processes. Journal of Pressure Vessel Technology, 133(6), 061205.

Diaz, O. G., Luna, G. G., Liao, Z., & Axinte, D. (2019). The new challenges of machining Ceramic Matrix Composites (CMCs): review of surface integrity. International Journal of Machine Tools and Manufacture.

Fang, Z., and Toshiyuki O. "Turning of Inconel 718 using inserts with cooling channels under high pressure jet coolant assistance." Journal of Materials Processing Technology 247 (2017): 19-28.

Folkes, J. "Waterjet—An innovative tool for manufacturing." Journal of Materials Processing Technology 209, no. 20 (2009): 6181-6189.

Hadavi, V., Michaelsen, B., Papini, M., 2015, Measurements and Modeling of Instantaneous Particle Orientation within Abrasive Air Jets and Implications for Particle Embedding. Wear, 336–337:9–20.

Han, W. and Fang, F., 2019. Fundamental aspects and recent developments in electropolishing. International Journal of Machine Tools and Manufacture, 139, pp.1-23.

He, Xingliang, Miao Song, Yao Du, Yi Shi, Blake A. Johnson, Kornel F. Ehmann, Yip-Wah Chung, and Q. Jane Wang. "Surface hardening of metals at room temperature by nanoparticle-laden cavitating waterjets." Journal of Materials Processing Technology 275 (2020): 116316.

Kong, M. C., and D. Axinte. "Response of titanium aluminide alloy to abrasive waterjet cutting: geometrical accuracy and surface integrity issues versus process parameters." Proceedings of the Institution of Mechanical Engineers, Part B: Journal of Engineering Manufacture 223.1 (2009): 19-42.

Kong, M. C., S. Anwar, J. Billingham, and D. A. Axinte. "Mathematical modelling of abrasive waterjet footprints for arbitrarily moving jets: part I—single straight paths." International Journal of Machine Tools and Manufacture 53, no. 1 (2012): 58-68.

Liao, Z., Axinte, D., Mieszala, M., M'Saoubi, R., Michler, J.,  Hardy, M., 2018. On the influence of gamma prime upon machining of advanced nickel based superalloy. CIRP Annals, 67(1), 109-112.

Liao, Z., Polyakov, M., Diaz, O.G., Axinte, D., Mohanty, G., Maeder, X., Michler, J. and Hardy, M., 2019a. Grain refinement mechanism of nickel-based superalloy by severe plastic deformation-Mechanical machining case. Acta Materialia, 180, pp.2-14.

Liao, Z., Abdelhafeez, A., Li, H., Yang, Y., Diaz, O. G., & Axinte, D. 2019b. State-of-the-art of surface integrity in machining of metal matrix composites. International Journal of Machine Tools and Manufacture.

Liu, H-T., Y. Hovanski, M. E. Dahl, and J. Zeng. "Applications of abrasive-waterjets for machining fatigue-critical aerospace aluminum parts." In ASME 2009 Pressure Vessels and Piping Conference, pp. 1-18. American Society of Mechanical Engineers Digital Collection, 2009.

Mieszala, M., P. Lozano Torrubia, Dragos A. Axinte, J. J. Schwiedrzik, Y. Guo, S. Mischler, J. Michler, and L. Philippe. "Erosion mechanisms during abrasive waterjet machining: model microstructures and single particle experiments." Journal of Materials Processing Technology 247 (2017): 92-102.

Melentiev R. and Fang F., "Recent advances and challenges of abrasive jet machining," CIRP Journal of Manufacturing Science and Technology, vol. 22, pp. 1-20, 2018.

Rivero, A., A. Alberdi, T. Artaza, L. Mendia, and A. Lamikiz. "Surface properties and fatigue failure analysis of alloy 718 surfaces milled by abrasive and plain waterjet." The International Journal of Advanced Manufacturing Technology 94, no. 5-8 (2018): 2929-2938.

Schwartzentruber, J., J. K. Spelt, and M. Papini. "Modelling of delamination due to hydraulic shock when piercing anisotropic carbon-fiber laminates using an abrasive waterjet." International Journal of Machine Tools and Manufacture 132 (2018): 81-95.

Shang, Z., Liao, Z., Sarasua, J.A., Billingham, J. and Axinte, D., 2019. On modelling of laser assisted machining: Forward and inverse problems for heat placement control. International Journal of Machine Tools and Manufacture, 138, pp.36-50.

Singh, J. and S.C. Jain, Mechanical Issues in Laser and Abrasive Water-Jet Cutting. Jom-Journal of the Minerals Metals & Materials Society, 1995. 47(1): p. 28-30.

Soyama, Hitoshi. "Comparison between the improvements made to the fatigue strength of stainless steel by cavitation peening, water jet peening, shot peening and laser peening." Journal of Materials Processing Technology 269 (2019): 65-78.

Tumbajoy-Spinel, David, Xavier Maeder, Gaylord Guillonneau, Sergio Sao-Joao, Sylvie Descartes, Jean-Michel Bergheau, Cécile Langlade, Johann Michler, and Guillaume Kermouche. "Microstructural and micromechanical investigations of surface strengthening mechanisms induced by repeated impacts on pure iron." Materials & Design 147 (2018): 56-64.

Ulutan, D. and Ozel, T., 2011. Machining induced surface integrity in titanium and nickel alloys: A review. International Journal of Machine Tools and Manufacture, 51(3), pp.250-280.

Wang, Z., Li, H.N., Yu, T.B., Wang, Z.X. and Zhao, J., 2019. Analytical model of dynamic and overlapped footprints in abrasive air jet polishing of optical glass. International Journal of Machine Tools and Manufacture, 141, pp.59-77.

Wei, H., Peng, C., Gao, H., Wang, X., & Wang, X. (2019). On establishment and validation of a new predictive model for material removal in abrasive flow machining. International Journal of Machine Tools and Manufacture, 138, 66-79.

Xu, D., Liao, Z., Axinte, D. and Hardy, M., 2020. A novel method to continuously map the surface integrity and cutting mechanism transition in various cutting conditions. International Journal of Machine Tools and Manufacture, 151, p.103529.